Supporting Information

Rafizadeh et al. 10.1073/pnas.1323541111

SI Materials and Methods

The human study protocol was approved by the University of California, Davis, Institutional Review Board. All animal care and procedures were approved by the University of California, Davis, Institutional Animal Care and Use Committee.

Yeast Two-Hybrid Screens. Yeast two-hybrid screening was performed with the GAL4 system by using the MATCHMAKER GAL4 Two-hybrid System 3 (Clontech) as we have described (1). AH109 was used as the yeast host strain. The SK2 baits in pGBKT7 vector were used to screen the human heart cDNA library of 3.5×10^6 clones in the pACT2 prey vector (Human Heart MATCHMAKER cDNA library catalog no. HL4042AH). Positive clones were selected by histidine and adenine prototrophy and assayed for α-galactosidase activity. Positive clones were isolated and characterized by sequencing.

Plasmid Construction. Human cardiac SK2 baits in pGBKT7 vector (Clontech) were used for yeast two-hybrid screen (Fig. 1*A*). Human cardiac SK2 baits were as followed: SK2-N, 1–145; SK2-M, 141–390; SK2-C1, 380–580; SK2-C2, 380–487; and SK2-C3, 481–580. The numbers refer to amino acid sequences according to human cardiac SK2 cDNA (GenBank accession no. AY258141). The cDNA fragments were placed in frame with the DNA binding domain (BD) of GAL4 by using PCR and subcloned into the pGBKT7 vector.

Human filamin A (FLNA) in pREP4 vector (Life Technologies) was a gift from Paramita M. Ghosh (University of California, Davis). α-actinin2 cDNA in pcDNA3 vector was a gift from D. Fedida (University of British Columbia, Vancouver) (2, 3). Construction of SK2 expression plasmids in a heterologous expression system, human embryonic kidney cells (HEK 293), was as follows: Full-length mouse cardiac SK2 cDNA was subcloned into pIRES2–EGFP (Clontech) to obtain pSK2–IRES–EGFP plasmid, and pSK2–IRES were generated by subcloning full-length SK2 cDNA into pIRES (Clontech). All of the above constructs were verified by sequencing.

HEK 293 Cells and Human Melanoma Cells (M2) Culture and Plasmids Transfection. HEK 293 cells or M2 cells (lacking the expression of FLNA) were maintained in DMEM supplemented with 10% (vol/vol) FBS, 100 U/mL penicillin, and 100 μg/mL streptomycin. The M2 cell line was a gift from J. H. Hartwig (Harvard Medical School, Boston). Cell lines were maintained at 37 °C in a humidified atmosphere containing 5% CO_2. All cell-culture reagents were purchased from Life Technologies. HEK 293 or M2 cells were transfected by using the following plasmid compositions: (*i*) pSK2–IRES–EGFP alone or in combination with (*ii*) pREP4–FLNA (1 μg for each plasmid) using Lipofectamine 2000 (Life Technologies) according to the manufacturer's protocol.

Antibodies. The following primary antibodies were used: (*i*) anti-SK2 antibody (Sigma-Aldrich; P0483), a polyclonal antibody raised in rabbits against a purified peptide corresponding to amino acid residues 542–559 of rat SK2 located in C terminus; (*ii*) monoclonal anti–α-actinin (sarcomeric) antibody (Sigma-Aldrich; A7811); (*iii*) anti-early endosomal antigen 1 (EEA1) antibody (610457; BD Biosciences); (*iv*) mouse monoclonal anti-FLNA antibody (Sigma; WH0002316M1) for immunofluorescence and rabbit monoclonal anti-FLNA antibody (Abcam; Ab76289) for Western blot analyses; and (*v*) Golgi Sampler Kit (BD Biosciences; 611434).

Secondary antibodies used were as follows: anti-mouse and -rabbit peroxidase-conjugated secondary antibodies (Calbiochem); goat anti-rabbit IgG–FITC conjugate (Sigma-Aldrich; F9887); goat polyclonal antibodies to mouse IgG–Texas Red conjugate (Abcam; ab6787); donkey anti-goat IgG–FITC conjugate; and goat anti-rabbit IgG–Rhodamine conjugate (Abcam).

Immunofluorescence Confocal Microscopy of Mouse Atrial Myocytes. Immunofluorescence labeling was performed as described (4). Cells were fixed by 4% paraformaldehyde in PBS for 30 min at room temperature, then washed with PBS for 5 min × 3, treated by 0.4% Triton X-100 in PBS for 15 min, washed and treated with −20 °C methanol for 10 min, and then washed and treated with antibody [1:100 dilution for anti-SK2 (Sigma-Aldrich) and 1:150 for anti-FLNA (Sigma) antibodies].

Immunofluorescence-labeled samples were examined by using Zeiss LSM700 confocal laser-scanning microscopy. For double staining, a secondary antibody-conjugated FITC was excited at 488 nm with the Ar laser and detected with a 505- to 530-nm bandpass filter, whereas conjugated Texas Red and Rhodamine were excited at 543 nm with the HeNe1 laser and detected at a 560-nm long-pass filter. To ascertain that there was no overlap between the detection of FITC and Texas Red or Rhodamine, singly labeled cells were imaged under identical conditions as those used for dual-labeled probes to confirm proper signal isolation of each channel. Control experiments performed by preincubation of the primary antibody with the respective antigenic peptide (1:1) did not show positive staining under the same experimental conditions used. Identical settings were used for all specimens.

Immunofluorescence Confocal Microscopy of HEK 293 Cells. HEK 293 cells were cotransfected with human cardiac SK2–HA channel together with α-actinin or FLNA by using Lipofectamine (Life Technologies; catalog no. 11668-019). Cells were treated with either vehicle or 25 μM, 2-Bis(2-aminophenoxy)ethane-*N*,*N*,*N*′,*N*′-tetraacetic acid tetraacetoxymethyl ester (BAPTA-AM) for 5 h before fixations with 4% paraformaldehyde. After blocking with 1% BSA (Sigma; catalog no. A7030) and no permeabilization, SK2 channels localized on the cell membrane were labeled with a monoclonal anti-HA antibody (Covance; catalog no. MMS-101P; 1:200 dilution) by incubating overnight in the humidified chamber (4 °C) followed by treatment with chicken anti-mouse Alexa Fluor 488 secondary antibody (Life Technologies; catalog no. A-21200; 1:500 dilution) for 1 h at room temperature. Cells were then permeabilized with 0.01% Triton X (Fisher) and blocked with 1% BSA again, and intracellular SK2 channels were labeled with anti-HA antibody (Covance; 1:500 dilution) at 4 °C overnight and a rabbit anti-mouse Alexa Fluor 555 secondary antibody (Life Technologies; catalog no. 21427; 1:500 dilution). Coverslips were mounted by using mounting medium containing DAPI (VectaMount; catalog no. H-5000; Vector Laboratories) and imaged under a Zeiss LSM 700 confocal laser-scanning microscope.

Specifically, to quantify the 488/555 fluorescence ratio, anti-HA antibody and Alexa Fluor 488 secondary antibody were used to label SK2 channel with extracellular HA tag (SK2–HA) before permeabilization. The cells were then permeabilized by using Triton X. Intracellular SK2 channels were then labeled with anti-HA antibody and Alexa Fluor 555 secondary antibody. The fluorescence ratio of 488/555 then represents the ratio of SK2 channel numbers on cell membrane over those inside the cells.

Control cells and BAPTA-AM–treated groups were immunolabeled in parallel, and all of the microscopic settings were kept the same between control and treated groups.

Western Blot Analysis. Protein samples were prepared from atria and ventricles of mice and human tissues. Human heart tissues were procured from a commercial source (T Cubed). Heart tissues were solubilized in ice-cold lysis buffer containing 50 mM Tris·HCl (pH 7.4), 1% Nonidet P-40, 1 mM EGTA, 0.15 M NaCl, 1 mM $MgCl_2$, and protease inhibitors, and then homogenized and centrifuged at 1,000 × *g* for 5 min at 4 °C to remove cell debris. Supernatant was collected to be analyzed by Western blot. Immunoblots were performed as described (1).

Site-Directed Mutagenesis. Point mutations were generated by using QuikChange Lightning Site-Directed Mutagenesis Kit (Stratagene; catalog no. 210518). The following primers were used:

pGBKT7–SK2-N P25A (P25A):

Forward, 5′- GGACTCCGAGGCTCAGGCCCTGCAGCCCCCCGCGTCC-3′;

Reverse, 5′- GGACGCGGGGGGCTGCAGGGCCTGAGCCTCGGAGTCC-3′;

pGBKT7–SK2-N P28A (P28A):

Forward, 5′-CCGAGGCTCAGCCCCTGGAGCCCCCCGCGTCCGTCG-3′;

Reverse, 5′-CGACGGACGCGGGGGGCTCCAGGGGCTGAGCCTCGG-3′;

pGBKT7–SK2-N 25PxxP28 double mutation to 25AxxA28 (P25A and P28A):

Forward, 5′-GGACTCCGAGGCTCAGGCCCTGGAGCCCCCCGCGTCC-3′;

Reverse, 5′-GGACGCGGGGGGCTCCAGGGCCTGAGCCTCGGAGTCC-3′;

pACT2–FLNA-C mut1(P2423A):

Forward, 5′-GATCCGAGTTGGGGAGGCTGGGCATGGAGGGGACCC-3′;

Reverse, 5′-GGGTCCCCTCCATGCCCAGCCTCCCCAACTCGGATC-3′;

pACT2–FLNA-C mut2 (P2457A):

Forward, 5′-GCCCTGTCGGTGACCATTGACGGCGCCTCCAAGGTGAAGATGGATTGCC-3′;

Reverse, 5′-GGCAATCCATCTTCACCTTGGAGGCGCCGTCAATGGTCACCGACAGGGC-3′;

pACT2–FLNA-C mut3 (P25A):

Forward, 5′-CCATCAAGTACGGCGGCGCCTACCACATTGGGGGCAGC-3′;

Reverse, 5′-GCTGCCCCCAATGTGGTAGGCGCCGCCGTACTTGATGG-3′;

pACT2–FLNA-C mut4

Forward, 5′-CCACATTGGGGGCAGCGCCTTCAAGGCCAAAGTCACAGG-3′;

Reverse, 5′-CCTGTGACTTTGGCCTTGAAGGCGCTGCCCCCAATGTGG-3′;

pACT2–FLNA-C mut5

Forward, 5′-CCAAGGCCACCTGTGCCGCCCAGCATGGGGCCCCGGG-3′;

Reverse, 5′-CCCGGGGCCCCATGCTGGGCGGCACAGGTGGCCTTGG-3′.

Patch–Clamp Recordings. Whole-cell Ca^{2+}-activated K^+ current ($I_{K,Ca}$) was recorded from transfected HEK 293 cells and neonatal mouse cardiomyocytes (NMCM) at room temperature by using conventional patch–clamp techniques as described (4, 5). The extracellular solution contained the following (in mmol/L): *N*-methylglucamine, 140; KCl, 4; $MgCl_2$, 1; glucose, 5; and Hepes, 10 (pH 7.4 using methane sulfonic acid). The internal solution consisted of the following (in mmol/L): K-gluconate, 144; $MgCl_2$, 1.15; EGTA, 5; Hepes, 10; and $CaCl_2$ yielding a free (unchelated) $[Ca^{2+}_i]$ of 500 nmol/L using Calcium Titration Software (6) to calculate free $[Ca^{2+}_i]$, bound and dissociated. The pH was adjusted to 7.25 by using KOH. The pipettes had resistances of 2–3 MΩ when filled with the pipette solution. Whole-cell $I_{K,Ca}$ was calculated as the apamin-sensitive component by using 100 pmol/L apamin. The cell capacitance was calculated by integrating the area under an uncompensated capacitive-transient elicited by a 20-mV hyperpolarizing pulse from a holding potential of −40 mV. Whole-cell current records were filtered at 2 kHz and sampled at 10 kHz. Liquid junction potentials were measured and corrected as described (7).

Mouse Neonatal Cardiomyocyte Isolation and Culture. To generate primary cardiomyocyte cultures, hearts were dissected from 1- to 2-d-old mouse pups. Cardiomyocytes were isolated and cultured as described (8). Protein and RNA were isolated from the cardiomyocytes at different time points and subjected to analysis by Western blotting, RT-PCR, and immunofluorescence confocal microscopy.

siRNA-Mediated Gene Knockdown. Mouse FLNA and GAPDH siRNA ON-TARGETplus Smart pool was purchased from Thermo Scientific. siGENOME Nontargeting pool #1 (Thermo Scientific) was used as a control. Mouse neonatal cardiomyoyctes grown to 80–90% confluency were transfected with 50 nmol/L pooled siRNA by using DharmaFECT I (Thermo Scientific) according to the manufacturer's instructions. Cells were used for experiments 48–72 h after transfection. The level of knockdown was quantified by real-time PCR. Total RNA was isolated by using TRIzol reagent (Life Technologies; 15596-026). RT-PCR was carried out by using SuperScriptIII first strand synthesis system (Life Technologies; 18080-051). cDNA was then used for real-time RT-PCR analysis with gene-specific primers. This protocol has been used by other groups to successfully knock down FLNA (9).

The sequences for the siRNAs used in the study were as follow:

ON-TARGETplus SMARTpool siRNA J-058520-17,

FLNA Target Sequence: GCUCAGAGGUAGACGUGGA

ON-TARGETplus SMARTpool siRNA J-058520-18,

FLNA Target Sequence: CCAGCAAGGUGAAGGCGUU

ON-TARGETplus SMARTpool siRNA J-058520-19,

FLNA Target Sequence: CAGAGUAACAGGUGACGAU

ON-TARGETplus SMARTpool siRNA J-058520-20,

FLNA Target Sequence: CAUUGAGGGUCCAUCUAAA.

Total Internal Reflection Fluorescence Microscopy. Human cardiac SK2 channel fused with tdTomato fluorescent protein and expressed in HEK 293 cells was used for total internal reflection

fluorescence microscopy (TIRF-M) to examine the effects of FLNA and α-actinin2 coexpression on the membrane expression of SK2 channels.

Computational Prediction of α-Actinin2 Bound to SK2 Channels. Based on our previously published data on the interaction site between the calmodulin (CaM)-binding domain (CaMBD) in the C terminus of SK2 channel and the second EF hand of α-actinin2 protein using site-directed mutagenesis and in vitro interaction assay (10), protein model visualization and analyses were performed by using the UCSF Chimera package (11). The final model for α-actinin2 bound to the CaMBD of SK2 channel was produced by a series of steps (Fig. S4). First, the CaMBD in the C terminus of SK2 channel bound to two molecules of calcified CaM was obtained from the published crystal structure [Protein Data Bank (PDB) ID code 1G4Y; Fig. S4*A*] (12). By using the matchmaker tool from the UCSF Chimera package, CaMBD of SK2 was superimposed onto the apoCaM bound to $Na_v1.5$ NMR structure (PDB ID code 2L53; Fig. S4*B*) (13). The resulting structure was then relaxed using the Rosetta (Version 3.4) Relax algorithm (Fig. S4*C*). α-actinin2 was then modeled after apoCaM by using the homology suite provided by Rosetta (Version 3.4) (14, 15), and the resulting structure was again relaxed (Fig. S4*D*). This structure was then superimposed onto the crystal structure of SK2 and calcified CaM (1G4Y) by using the matchmaker tool provided by the UCSF Chimera package and analyzed visually. Indeed, the resultant molecular structure (Fig. S4*E*) is in excellent agreement with our previously published mutagenesis data (10).

Data Analysis. Curve fits and data analysis were performed by using Origin software (MicroCal). Current density obtained from cells expressing SK2 alone or in combination with FLNA was compared by normalizing the currents with cell capacitance. Where appropriate, pooled data are presented as means ± SEM. Statistical comparisons were performed by using the statistical package in the Origin software with $P < 0.05$ considered significant. For multiple comparisons, one-way analysis of variance combined with Dunnett's test was used.

1. Lu L, et al. (2007) Molecular coupling of a Ca^{2+}-activated K^+ channel to L-type Ca^{2+} channels *via* α-actinin2. *Circ Res* 100(1):112–120.
2. Cukovic D, Lu GW, Wible B, Steele DF, Fedida D (2001) A discrete amino terminal domain of Kv1.5 and Kv1.4 potassium channels interacts with the spectrin repeats of alpha-actinin-2. *FEBS Lett* 498(1):87–92.
3. Maruoka ND, et al. (2000) alpha-actinin-2 couples to cardiac Kv1.5 channels, regulating current density and channel localization in HEK cells. *FEBS Lett* 473(2):188–194.
4. Xu Y, et al. (2003) Molecular identification and functional roles of a Ca^{2+}-activated K^+ channel in human and mouse hearts. *J Biol Chem* 278(49):49085–49094.
5. Hamill OP, Marty A, Neher E, Sakmann B, Sigworth FJ (1981) Improved patch-clamp techniques for high-resolution current recording from cells and cell-free membrane patches. *Pflugers Arch* 391(2):85–100.
6. Robertson S, Potter JD (1984) The regulation of free Ca^{2+} ion concentration by metal chelators. *Myocardial Biology*, Methods in Pharmacology, ed Schwartz A (Plenum, New York), pp 63–75.
7. Neher E (1992) Correction for liquid junction potentials in patch clamp experiments. *Methods Enzymol* 207:123–131.
8. Xu Y, et al. (2005) The effects of intracellular Ca^{2+} on cardiac K^+ channel expression and activity: Novel insights from genetically altered mice. *J Physiol* 562(Pt 3):745–758.
9. Minsaas L, et al. (2010) Filamin A binds to CCR2B and regulates its internalization. *PLoS ONE* 5(8):e12212.
10. Lu L, et al. (2009) Alpha-actinin2 cytoskeletal protein is required for the functional membrane localization of a Ca^{2+}-activated K^+ channel (SK2 channel). *Proc Natl Acad Sci USA* 106(43):18402–18407.
11. Pettersen EF, et al. (2004) UCSF Chimera—a visualization system for exploratory research and analysis. *J Comput Chem* 25(13):1605–1612.
12. Schumacher MA, Rivard AF, Bächinger HP, Adelman JP (2001) Structure of the gating domain of a Ca^{2+}-activated K^+ channel complexed with Ca^{2+}/calmodulin. *Nature* 410(6832):1120–1124.
13. Chagot B, Chazin WJ (2011) Solution NMR structure of apo-calmodulin in complex with the IQ motif of human cardiac sodium channel $Na_v1.5$. *J Mol Biol* 406(1):106–119.
14. Raman S, et al. (2009) Structure prediction for CASP8 with all-atom refinement using Rosetta. *Proteins* 77(Suppl 9):89–99.
15. Chivian D, Baker D (2006) Homology modeling using parametric alignment ensemble generation with consensus and energy-based model selection. *Nucleic Acids Res* 34(17):e112.

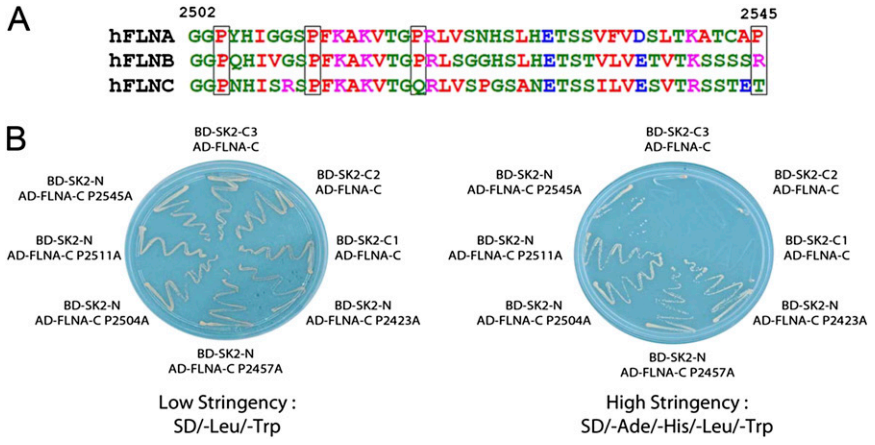

Fig. S1. The C terminus of FLNA directly interacts with the SK2 N terminus, but not the SK2 C terminus. (*A*) Amino acid sequence alignment for the C-terminal fragments of human FLN A, B, and C (hFLNA, hFLNB, and hFLNC, respectively) highlighting the proline residues in hFLNA. Ten single-point mutations of proline to alanine were constructed in FLNA-C. A mutation of proline at position 2,545 to alanine (FLNA-C P2545A) resulted in a decrease in the number of colonies under high-stringency conditions (see *B*). (*B*) Different regions of human cardiac SK2 channel (Fig. 1*A*) in pGBKT7 vector (BD vector) were used as baits for the yeast two-hybrid assay including BD–SK2-N, BD–SK2-C1, BD–SK2-C2, and BD-SK2-C3. Interaction between BD–SK2-N and the C-terminal 385 amino acids of FLNA in pACT2 vector [activating domain (AD) vector, AD-FLNA-C] was confirmed three times by using the yeast-two-hybrid assay depicted as growth of colonies in a high-stringency medium (SD/-Ade/-His/-Leu/-Trp; *Right*). In contrast, there were no interactions between AD–FLNA-C and the C-terminal domain of the SK2 channel (BD–SK2-C1, BD–SK2-C2, or BD–SK2-C3). Ten single-point mutations of proline to alanine were generated in AD–FLNA-C. A mutation of proline at position 2,545 to alanine (AD–FLNA-C P2545A) resulted in a decrease in the number of colonies under high-stringency conditions (*Right*).

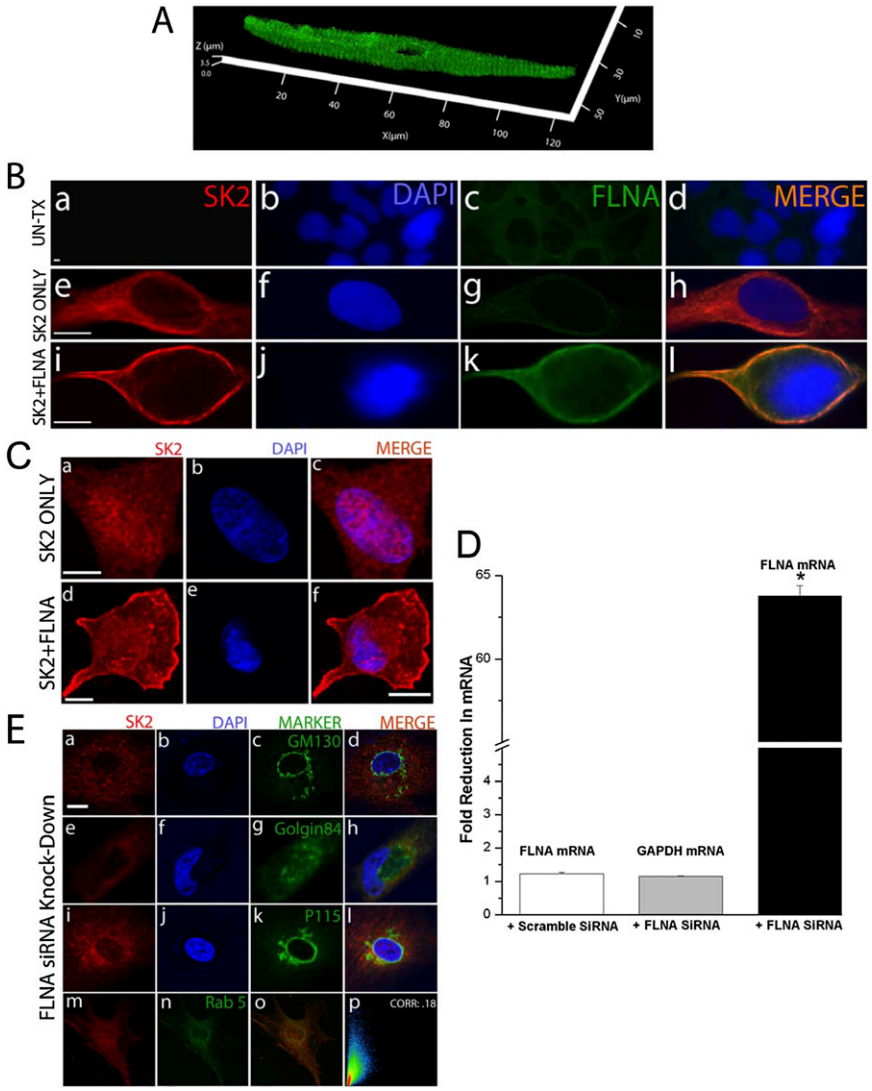

Fig. S2. Expression of FLNA enhances the membrane localization of SK2 channel proteins in HEK 293 cells and FLNA-deficient M2 cells, and siRNA knockdown of FLNA diminishes membrane localization of SK2 in NMCMs. (*A*) Immunofluorescence confocal microscopic image of Z-stack reconstruction using anti-FLNA antibody depicting FLNA localization along Z lines. (*B*, *a–d*) Immunofluorescence confocal microscopic images from nontransfected (UN-TX) HEK 293 cells showing no SK2 channel expression and a basal level of FLNA protein. (*B*, *e–h*) HEK 293 cells transfected with SK2 channel alone showing SK2 localization mainly in the intracellular compartments. (*B*, *i–l*) HEK 293 cells coexpressing SK2 and FLNA showing an increase in SK2 channel protein on the plasma membrane. (Scale bars, 10 μm.) (*C*, *a–c*) Immunofluorescence confocal microscopic images from FLNA-deficient M2 cells transfected with SK2 only, showing SK2 localization mainly in the intracellular compartments. (*C*, *d–f*) M2 cells were cotransfected with SK2 and FLNA showing a significant increase in SK2 protein plasma membrane localization. (Scale bars, 10 μm.) (*D*) Summary data from real-time RT-PCR confirming the knockdown of FLNA in NMCMs. A nontargeting siRNA (column 1) did not alter FLNA mRNA expression, whereas a specific anti-FLNA siRNA (column 3) did. Anti-FLNA siRNA did not alter GAPDH mRNA expression (column 2). Experiments were performed in triplicate. $*P < 0.05$. (*E*) Immunofluorescence confocal microscopic images from NMCMs treated with FLNA siRNA immunostained with anti-SK2 antibody and antibodies directed against intracellular organelles including anti-GM130, -Golgin84, -P115, and -Rab5 antibodies. siRNA knockdown of FLNA protein significantly reduced SK2 channel proteins localization on the plasma membrane. The scatter plot in *p* shows a poor correlation between SK2 channels and Rab5. All pixels in the images have been assigned a position on the scatter plots and are placed according to the intensity of red or green signals. Colocalization analysis shows a correlation coefficient of 0.18. (Scale bar, 10 μm.)

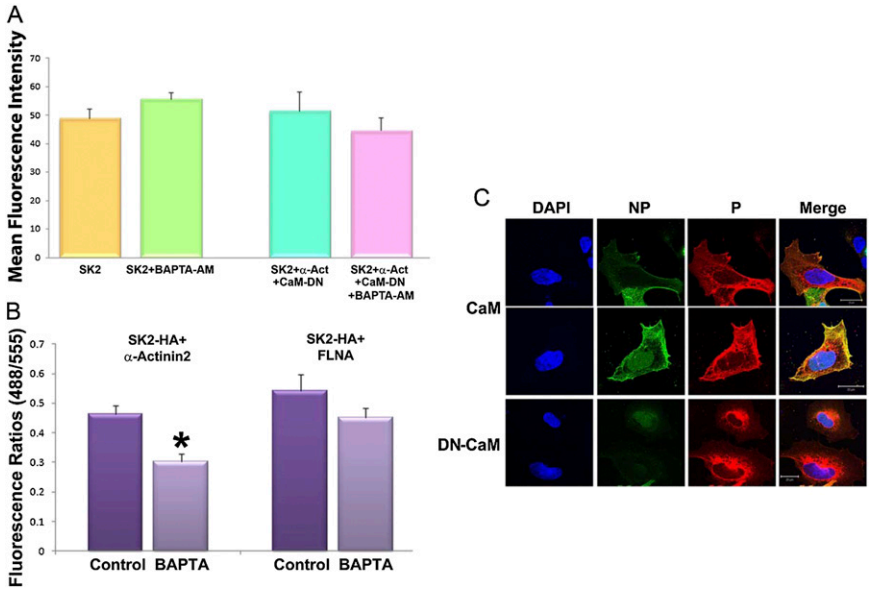

Fig. S3. Endogenous CaM or α-actinin2 alone does not suffice to confer Ca^{2+} sensitivities to the trafficking of SK2 channels. (*A*) Summary data of fluorescence intensity in the TIRF mode showing no significant changes in the fluorescence intensity in cells expressing SK2 alone or SK2, α-actinin2, and DN-CaM after pretreatment with BAPTA-AM. *P* was not significant ($n = 8$ cells per group). (*B*) Summary data of the fluorescence ratios (488/555) from the four groups of cells in Fig. 7 *A* and *B*. $*P < 0.0004$ ($n = 16$–20 cells). There was a significant decrease in the fluorescence ratios (488/555) in HEK 293 cells coexpressing SK2 and α-actinin2 treated with BAPTA-AM compared with control. In contrast, no significant differences were observed in cells coexpressing SK2 and FLNA with or without BAPTA-AM pretreatment. (*C*) Control experiments were performed by using HEK 293 cells cotransfected with wild-type CaM (CaM) or dominant-negative CaM (DN-CaM). (Scale bar, 20 μm.)

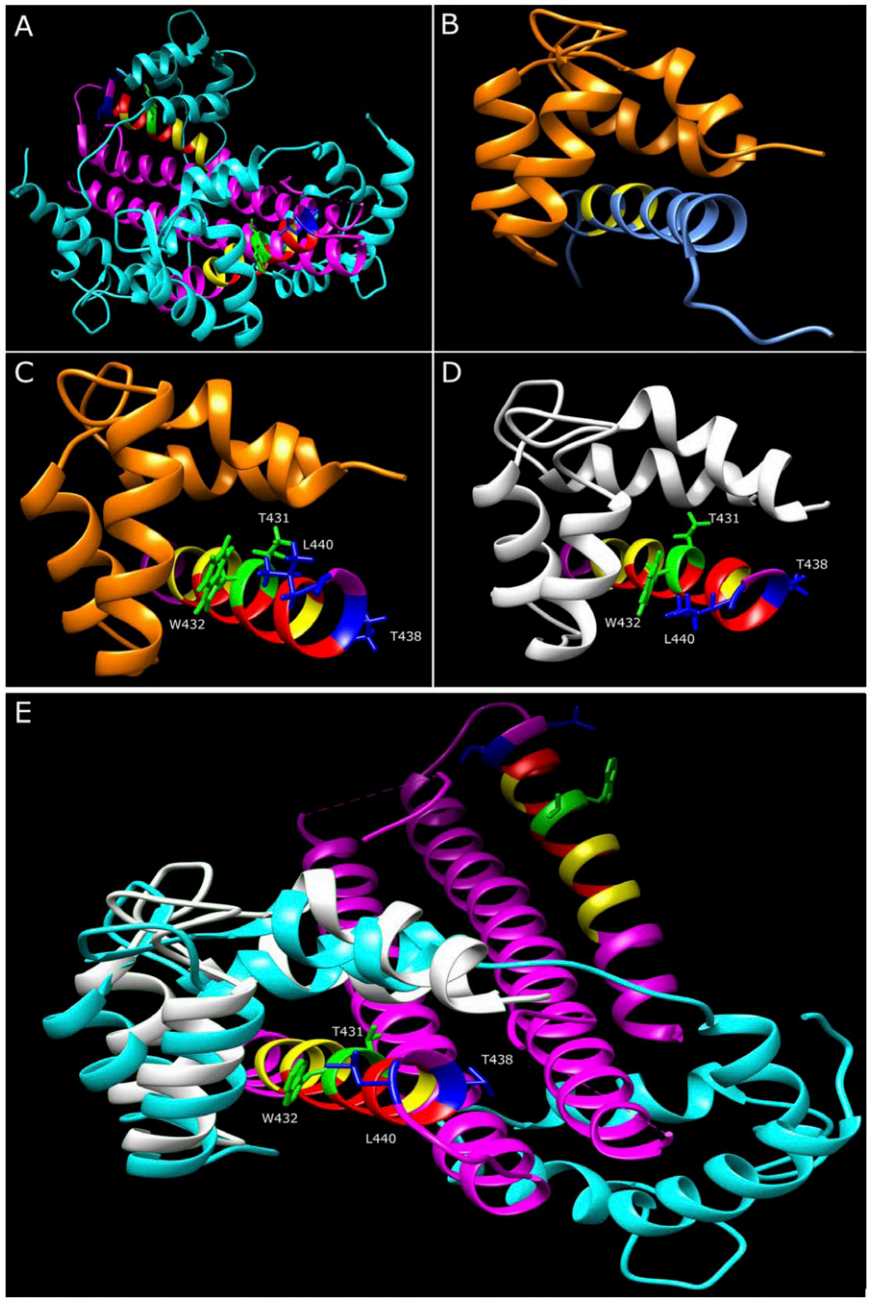

Fig. S4. Computational prediction of α-actinin2 bound to SK2. (*A*) A crystal structure of CaM bound to the SK2 C terminus from published literature (PDB ID code 1G4Y). Two molecules of calcified CaM are represented by the cyan structure bound to the C termini of two different subunits of SK2 channels (purple structure). The amino acids colored in red represent the CaMBD, and the amino acids colored in yellow represent highly conserved hydrophobic amino acids. The amino acids colored in green represent residues (T431, W432) within the CaMBD that we have previously shown to be critical for protein interaction with α-actinin2 protein. The dark blue amino acids represent amino acid residues outside of the CaMBD (T438, L440), which we have previously mutated. Mutations of these residues did not affect the interaction of SK2 C terminus and α-actinin2 in our study. (*B*) Published NMR structure of apoCaM (orange structure) bound to $Na_v1.5$ (light blue structure; PDB ID code 2L53). The yellow amino acids represent the conserved hydrophobic amino acids. (*C*) Region of $Na_v1.5$ from *B* replaced by the CaMBD from SK2 channel, coloring of amino acids as in *A*. (*D*) ApoCaM in *C* was replaced by α-actinin2 (white model), coloring of amino acids as in *A*. (*E*) The crystal structure as presented in *A* with one CaM molecule replaced by α-actinin2 from previous image.